Tuning depth profiles of organosilicate films with ultraviolet curing

Taek-Soo Kim,[1] Naoto Tsuji,[2] Kiyohiro Matsushita,[2] Nobuyoshi Kobayashi,[2] Dmytro Chumakov,[3] Holm Geisler,[3] Ehrenfried Zschech,[3] and Reinhold H. Dauskardt[4,a)]
[1]*Department of Mechanical Engineering, Stanford University, Stanford, California 94305, USA*
[2]*ASM Japan K.K., 23-1, 6-chome Nagayama, Tama-shi, Tokyo, 206-0025, Japan*
[3]*AMD Fab36 LLC and Co. KG, Wilschdorfer Landstrasse 101, Dresden, Saxony, 01109, Germany*
[4]*Department of Materials Science and Engineering, Stanford University, Stanford, California 94305, USA*

(Received 8 July 2008; accepted 22 August 2008; published online 14 October 2008)

This study demonstrates that ultraviolet (UV) radiation curing can control depth profiles of organosilicate films. Striking differences between the effects of monochromatic and broadband UV irradiation were observed. For the same as-deposited organosilicate film and cure duration, monochromatic radiation has a greater impact on film structure, elastic modulus, and fracture resistance, but also results in a greater degree of depth dependent properties. Oscillating elastic modulus through the film thickness was observed with force modulation atomic force microscopy. We present a new standing wave model that accurately predicts the resulting depth dependent stiffness variations considering changes in film shrinkage and refractive index in terms of curing time, and can further be used to account for initial film thickness dependence of UV curing and film absorption. Promising applications of the depth dependent UV curing to produce multifunctional ultralow-*k* layers with a single postdeposition curing process are discussed. © *2008 American Institute of Physics*. [DOI: 10.1063/1.2999637]

I. INTRODUCTION

We recently reported depth dependence of UV curing of a series of experimental organosilicate low-*k* thin film glasses, which has implications for the variation in mechanical properties through the thickness of the films.[1,2] Specifically, an oscillating elastic modulus depth profile following UV cure was measured by force modulation atomic force microscopy (FM-AFM). The oscillation was associated with UV light interference, which we modeled using a modification of the Cuthbert standing wave equation.[2] However, such models suggest that changes in film shrinkage and refractive index in terms of curing time are important variables that must be included, which has not been accounted for in recent work.[2,3]

In this study we present a new standing wave model that accurately predicts the resulting depth dependent stiffness variations considering changes in film shrinkage and refractive index in terms of curing time, and can further be used to account for initial film thickness dependence of UV curing and film absorption. Organosilicate films deposited on silicon substrates and cured with monochromatic and broadband UV irradiations, respectively, were examined. Significant differences between the effects of monochromatic and broadband UV irradiations were observed. For the same as-deposited organosilicate films and cure duration, monochromatic radiation had a greater impact on film structure, elastic modulus, and fracture resistance, but also resulted in a higher degree of depth dependent properties. Oscillating elastic modulus through the film thickness was observed with FM-AFM. We also demonstrate that initial film thickness can have a significant effect on the stiffness cure profile, and further that broadband sources containing multiple peaks can also result in significant depth dependent cure.

II. EXPERIMENTAL

Experimental organosilicate films with thickness of 500 nm were deposited by plasma enhanced chemical vapor deposition (PE-CVD) onto silicon wafers. After deposition, they were exposed to monochromatic UV radiation with a wavelength $\lambda < 200$ nm and broadband UV radiation with $\lambda > 200$ nm, respectively, for selected curing durations in a controlled environment. Following the UV cure, material properties of the organosilicate films were measured and the films were capped with 100 nm thick PE-CVD SiCN barrier layers. The measured material properties of the films are summarized in Table I. The film thickness and density were measured by spectroscopic ellipsometry and x-ray reflectivity, respectively. The elastic modulus and hardness were measured by nanoindentation with indentation depths of 20–30 nm and 90–100 nm, respectively.

The FM-AFM technique was used to investigate the variations in the elastic modulus on the cross section of specimens containing UV cured 500 nm organosilicate films. Two thin film structures were bonded with epoxy, and the specimen consisting of the two thin film structures was diced and polished by chemical mechanical planarization (CMP) to produce a flat cross section. During FM scans on the cross section the AFM tip always remained in contact with the surface. The quantitative estimation of the elastic modulus is based on the modeling of the mechanics of the tip-specimen elastic interaction. The calculations rely on Hertzian contact theory[4] to consider the deformation of both the surface and the tip. The present FM-AFM measurements require the knowledge of the reduced modulus at any two locations on

a)Electronic mail: dauskardt@stanford.edu.

TABLE I. Material properties of the initially 500 nm thick organosilicate films UV-cured for various curing durations.

UV type	Curing time t (a.u.)	Dielectric constant k	Index of refraction n	Elastic modulus E (GPa)	Hardness H (GPa)	Density ρ (g cm^{-3})	Residual film stress σ_f (MPa)	Film shrinkage S (%)
Pristine	0	2.71	1.3553	5.27 ± 0.11	0.93 ± 0.02	1.199	55.11	0
Monochromatic	2	2.69	1.3658	10.68 ± 0.13	1.85 ± 0.04	1.256	76.3	8.50
	5	2.79	1.3807	16.03 ± 0.40	2.54 ± 0.05	1.283	105.7	14.05
	10	3.02	1.3933	22.44 ± 0.54	3.11 ± 0.06	1.360	118.4	18.03
Broadband	2	2.64	1.3551	6.04 ± 0.17	1.09 ± 0.04	1.252	55.9	1.72
	4	2.65	1.3552	6.77 ± 0.14	1.24 ± 0.01	1.253	56.2	2.92
	10	2.68	1.3552	7.86 ± 0.20	1.47 ± 0.03	1.278	59.1	4.80
	20	2.72	1.3556	8.65 ± 0.18	1.62 ± 0.03	1.312	60.2	6.78

the sample that possesses different elastic modulus values. These values are needed for the calibration of tip and cantilever parameters that play a determinant role in delivering the quantitative information. The corresponding calibration was performed by using a nanoindentation tool with *in situ* scanning probe microscopy imaging capability on sample regions, which are still large enough to be measured with the tip of the nanoindenter.

Four-point bend (FPB) and double cantilever beam (DCB) specimen geometries were fabricated for fracture energy and crack-growth testing by sandwiching the films between two elastic silicon substrates using previously reported epoxy bonding techniques.[5] The interface fracture energy near the top or bottom of the organosilicate films was measured using the FPB technique[6] with inner and outer pin spacing of 27 and 40 mm, respectively, and a constant displacement rate of 0.5 μm s^{-1}. The fracture location was determined by notching in either side of the FPB specimen. The cohesive fracture energy was measured by the DCB technique.[7] Cracks were introduced in the organosilicate film using a prenotch in the DCB specimen and loading until fracture initiated. The DCB test configuration typically produces cohesive fracture in the center of the brittle organosilicate layer, which was observed for all tests conducted. Crack growth rates da/dt were characterized as a function of the applied strain energy release rate G(J m^{-2}) over the range of 10^{-4} m s^{-1} to approximately 10^{-10} m s^{-1} using load relaxation fracture mechanics techniques with the DCB specimens.[8] This involved loading the specimen at a constant displacement rate to a predetermined load then fixing the displacement. The following time-dependent load relaxation resulting from crack growth increases the specimen compliance from which the crack length, a, da/dt, and G may be determined. Tests were conducted in an environmental chamber with temperature and humidity control of 30 ± 0.5 °C and $50 \pm 1\%$ relative humidity, respectively. After testing, the specimens were examined using high resolution x-ray photoelectron spectroscopy to determine the fracture path in the thin-film structures. Spot size of 150×1000 μm was used to perform survey scans for the binding energy range of 0–1000 eV.

III. RESULTS AND DISCUSSION

Monochromatic UV curing resulted in drastic improvement in elastic modulus compared to broadband UV curing with cure time as shown in Fig. 1(a). Following the same curing time UV × 10 (ten times a selected curing duration in arbitrary unit), monochromatic UV curing increased elastic modulus by 330%, whereas broadband UV curing increased it by 50%. However, monochromatic UV curing also incurred significant increase in dielectric constant, shrinkage of film thickness, and refractive index [Figs. 1(b)–1(d)]. Fourier transform infrared spectroscopy spectra showed that monochromatic UV curing significantly reduces the Si–CH_3 terminal group and increases Si–O network bonds, whereas minor decrease in the Si–CH_3 terminal group occurred for broadband UV curing.[9] As shown in Figs. 2(a) and 2(b), the fracture resistance at the top of the UV-cured organosilicate layers was found to increase significantly with cure time, 490% by the monochromatic and 40% by the broadband UV × 10 curing. However, the fracture resistances at the middle and bottom of the organosilicate layers were relatively insensitive to the UV curing. Moreover, moisture-assisted crack growth behaviors of the UV cured organosilicate layers were identical or have the same threshold value of applied strain energy release rate except for the monochro-

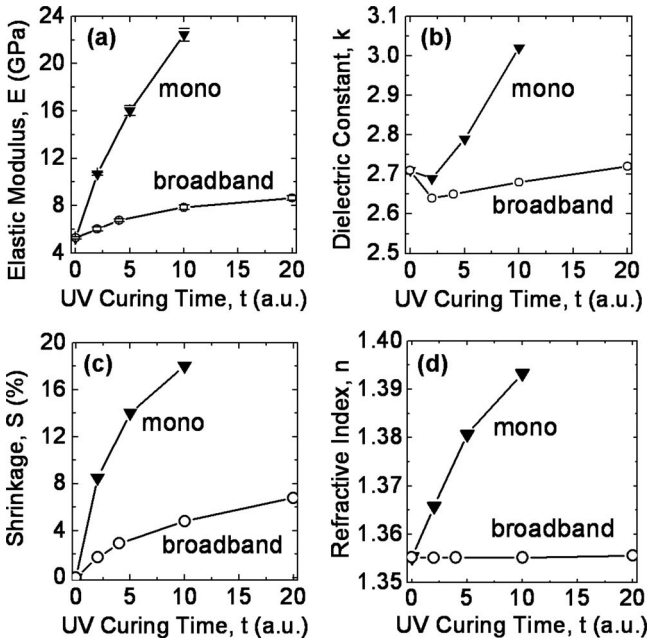

FIG. 1. Materials properties are plotted in terms of UV curing time for (a) elastic modulus, (b) dielectric constant, (c) shrinkage of film thickness, and (d) refractive index.

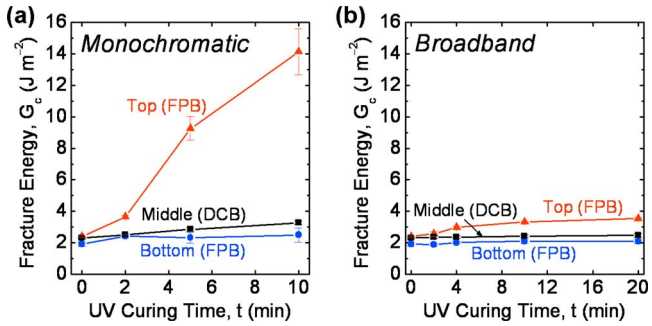

FIG. 2. (Color online) Fracture energies of organosilicate layers cured by (a) monochromatic and (b) broadband UV irradiations. Interface fracture energies near the top and bottom of the organosilicate films were measured by the FPB technique, and the cohesive fracture energies near the middle of the films were measured by the DCB technique.

matic UV × 10 curing [Figs. 3(a) and 3(b)]. This means that the bond density at the crack tip and the reactivity of the crack tip bonds to the moist air did not change much following the UV curing. The crack tip in a DCB configuration might avoid newly formed bonds occurring by UV cure, resulting in little effect on the cohesive fracture energy.[10,11]

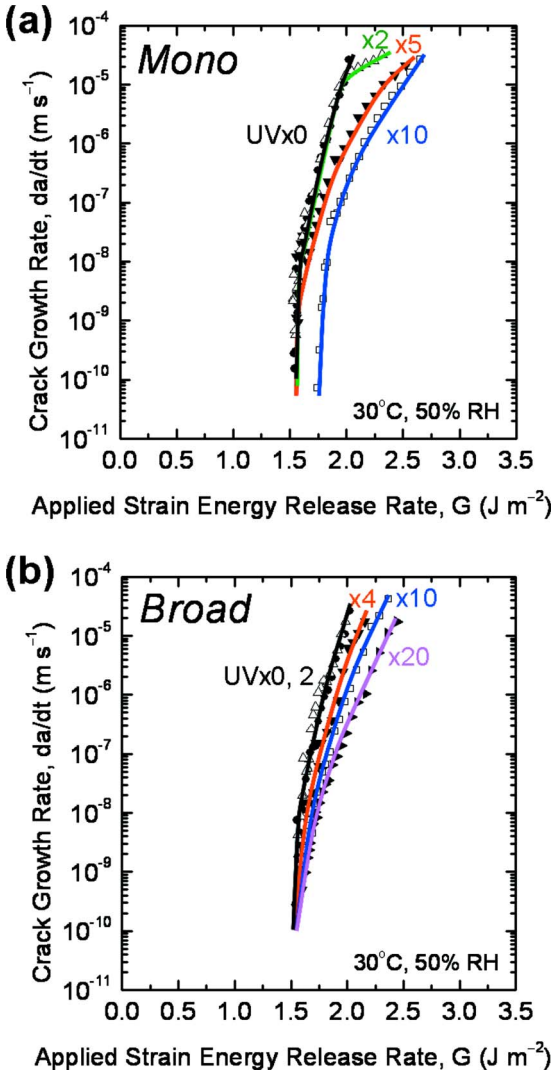

FIG. 3. (Color online) Moisture-assisted cracking of organosilicate layers cured by (c) monochromatic and (d) broadband UV irradiations.

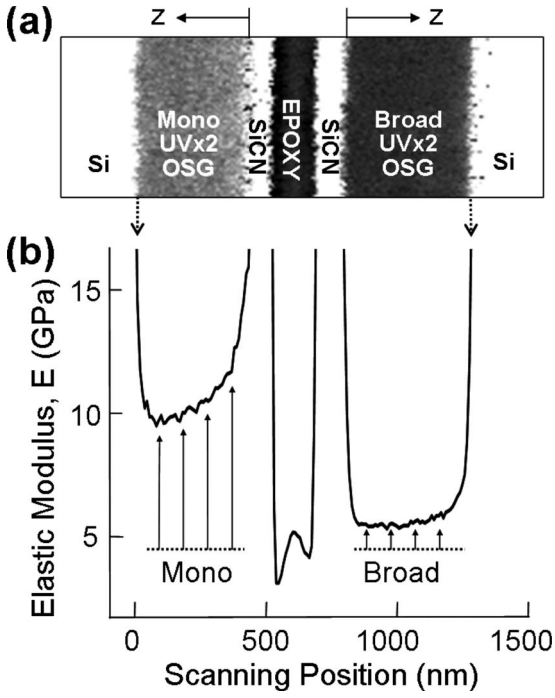

FIG. 4. (a) The FM signal image of a cross section of a specimen containing monochromatic and broadband UV × 2 cured organosilicate films. (b) Measured elastic modulus variations in the UV × 2 cured films are plotted in terms of the scanning position. The dashed line represents the elastic modulus of the uncured organosilicate layer measured by FM-AFM.

The crack path selection, however, does not appear enough to explain the insensitivity of the cohesive fracture resistance to the monochromatic UV curing that increased the fracture energy and elastic modulus at the top of the organosilicate films up to 490% and 330%, respectively.

Note that the fracture energy measured at the top of the monochromatic UV × 10 cured film is well in excess of the fracture energy of fully dense silica ($G_c \sim 10$ J/m^2).[12] This suggests that material at the top of the layer has become densified during curing resulting in the large fracture energy and that this higher inherent fracture resistance results in other forms of energy dissipation. These may include plastic energy dissipation in the epoxy bond layer adjacent to the SiCN layer, although these effects are thought to be minimal since a thin Cr/Al layer was employed in the sample preparation that together with the SiCN layer would provide an elastic standoff layer reducing stresses in the epoxy bond layer. Frictional contact associated with debond surface roughness may also contribute, but again no evidence for increased roughness for these samples have been observed.

Striking differences between the effects of monochromatic and broadband UV irradiations on elastic modulus were revealed by FM-AFM (Fig. 4). A typical FM signal image of a cross section of the specimen containing two organosilicate layers UV × 2 cured with monochromatic and broadband irradiation, respectively, is shown in Fig. 4(a). The variation in the elastic modulus was measured through the initially 500 nm organosilicate films UV × 2 cured with monochromatic and broadband irradiation, respectively, and plotted as a function of the horizontal scanning position in Fig. 4(b). The increment in elastic modulus by the mono-

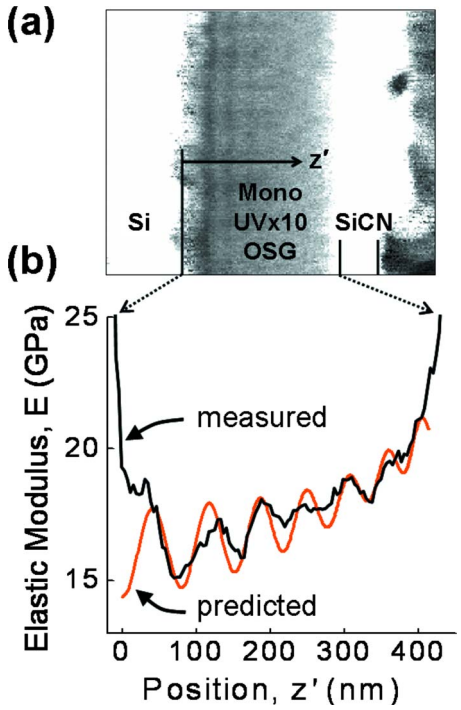

FIG. 5. (Color online) (a) The FM signal image of a cross section of a specimen containing a monochromatic UV×10 organosilicate film. (b) An elastic modulus depth profile of the monochromatic UV×10 film measured by FM-AFM is compared with predicted one by the standing wave simulation.

chromatic irradiation is not only greater than that by the broadband but also depth dependent through the film thickness, while the increased elastic modulus by the broadband is uniform through the film thickness. The increment in elastic modulus is more than 100% at the top of the organosilicate layer where it is irradiated by the monochromatic UV light. However, it attenuates exponentially with film depth z. The differences between the monochromatic and the broadband are largely due to wavelength-dependent absorption in which the absorption coefficient of the light-absorbing layer increases precipitously with UV light with a shorter wavelength ($\lambda < 200$ nm).[13] An empirical relationship of the light absorption and the material properties through which the light is propagating is given by Beer–Lambert law

$$I = I_o \exp(-\alpha z), \tag{1}$$

where I is light intensity at the film depth of z, I_o is incident light intensity, and α is absorption coefficient of the organosilicate film. Figure 4(b) clearly shows that the organosilicate film has high α with the monochromatic UV ($\lambda < 200$ nm) and low α with the broadband UV ($\lambda > 200$ nm).

Even astonishing finding with the FM-AFM stiffness map is the oscillation of the elastic modulus through the film thickness of the monochromatic cured organosilicate film (Fig. 5). Even though the amplitude of the oscillation was small for the shorter cure time (UV×2), it was significantly larger for the longer cure time (UV×10), as shown in Fig. 5(b). The oscillation was so obvious that the modulus variations appeared visually as ripples parallel to the film plane in the FM signal image [Fig. 5(a)].

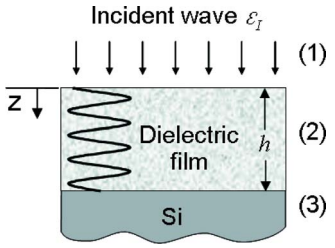

FIG. 6. (Color online) Geometry used in the derivation of the standing wave model.

As we reported previously, the oscillation of the elastic modulus following UV cure is associated with UV standing wave effects.[2] Standing waves caused by UV light interference are an undesirable side effect of the exposure process in optical lithography, which leads to severe variations in light intensity perpendicular to the resist film.[14–17] We previously used a simple equation of Cuthbert model for the formation of a standing wave. In the present paper, we develop a new general formulation based on the Mack model that will allow us to include the changes in film thickness, refractive index, and absorption. When a thin dielectric film placed between two semi-infinite media (e.g., a thin coating between a vacuum and a reflecting substrate) is exposed to monochromatic light, standing waves are produced in the film, as shown in Fig. 6.[14] The electric field of the standing waves within a thin film [region (2) in Fig. 6] can be analytically expressed as

$$\varepsilon_2(z) = \varepsilon_I \tau_{12} \frac{\exp(-ik_2 z) + \rho_{23}\tau_h^2 \exp(ik_2 z)}{1 + \rho_{12}\rho_{23}\tau_h^2}, \tag{2}$$

and the standing wave intensity in the thin film is

$$I_2(z) = |\varepsilon_2(z)|^2, \tag{3}$$

where ε_I is the incident wave at $z=0$, $\rho_{ij}=(\mathbf{n}_i-\mathbf{n}_j)/(\mathbf{n}_i+\mathbf{n}_j)$ is the reflection coefficient, $\tau_{ij}=2\mathbf{n}_i/(\mathbf{n}_i+\mathbf{n}_j)$ is the transmission coefficient, $\tau_h=\exp(-ik_2 h)$ is the internal transmittance of the thin film, $k_j=2\pi\mathbf{n}_j/\lambda$ is the propagation constant, $\mathbf{n}_j=n_j-i\kappa_j$ is the complex index of refraction, and κ_j is the extinction coefficient.[14] Note that the propagation of an electric field through some material can implicitly account for absorption by using a complex index of refraction $\mathbf{n}$ for the material. The imaginary part of the index of refraction is related to the absorption coefficient by $\alpha=4\pi\kappa/\lambda$. Therefore Eq. (1) is implied in the standing wave model [Eq. (2)].

Assuming the UV cure intensity is proportional to the light intensity, the increment in elastic modulus at the film depth of z following the curing duration t_{final} is proportional to the integration of Eq. (3) from $t=0$ to $t=t_{\text{final}}$. However, to account for the shrinking film thickness $h(t)=h_o(1-S(t)/100)$, where h_o is the initial film thickness of 500 nm and refractive index $n(t)$, their experimental data were curve fitted and substituted in Eq. (2). The resulting UV cure intensity U in terms of the film depth z following cure duration t is then

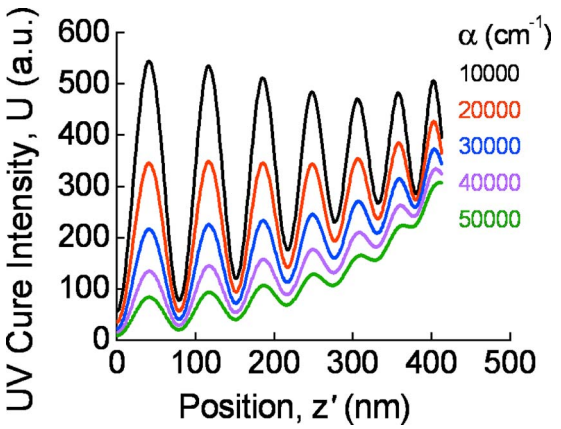

FIG. 7. (Color online) UV cure intensity depth profiles plotted with selected values of the absorption coefficient α.

$$U(z,t) = \int_0^t I_2[h(t),n(t),z]dt. \tag{4}$$

The UV cure intensity depth profiles are plotted with selected values of the absorption coefficient in Fig. 7. Note that the UV cure intensity depth profiles are dominated by the standing wave effect with the lower absorption coefficients or by the light absorption effect with the higher absorption coefficients. With lower absorption coefficients, the oscillation of UV cure intensity is severer but the average value of that is relatively uniform compared to that with higher absorption coefficients through the film thickness due to the strong standing wave formation and weak absorption through the film thickness. On the contrary, with higher absorption coefficients, the oscillation is relatively small but the average value decays exponentially with the film depth, which is characteristic of the Beer–Lambert law of absorption.

Correlation between the UV cure intensity $U(z,t)$ and a resulting elastic modulus E has not been formally established. However, based on the effect of UV curing on a resulting elastic modulus value we suggest a new model to account for the effects of $U(z,t)$ on a local elastic modulus E in terms of the film depth z following cure duration t as follows:

$$E(z,t) = \Phi(z,t)U(z,t) + E_o, \tag{5}$$

where E_o is the initial elastic modulus and Φ is a photochemical parameter that involves the quantum efficiency of photons used to remove terminal bonds such as Si–OH and Si-CH_3 and leads to a subsequent formation of cross-linking Si–O–Si bonds resulting in the increase in E. Φ can be estimated from measured mechanical and optical properties in Fig. 1. The elastic modulus E simulated by the standing wave model is plotted and compared with the AFM stiffness map, as shown in Fig. 5(b). The model prediction matches observed variations with surprising accuracy, which certainly implies that the depth dependent UV curing is caused by UV standing wave effects that we analytically predicted. The predicted absorption coefficient α is 35 000 cm^{-1} and this value is close to the measured one by nitrogen-purged ultraviolet spectroscopic ellipsometry.[3]

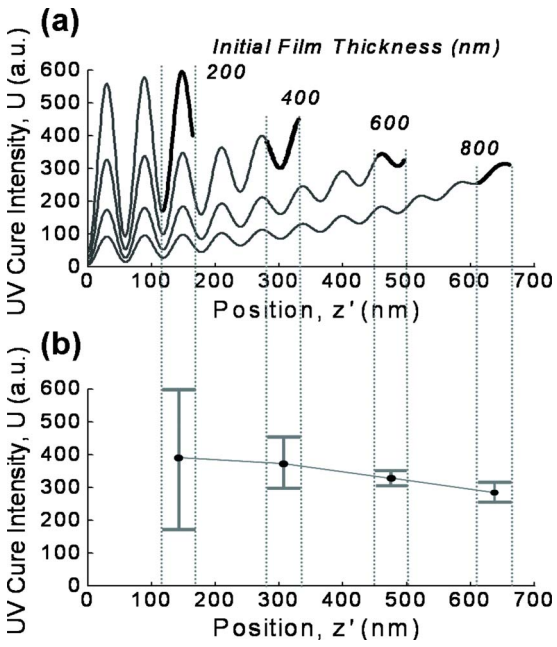

FIG. 8. (Color online) (a) Model predictions of the UV cure depth profiles of organosilicate films with a various initial thickness. Bold solid lines are UV cure profiles at the upper part of the films within 50 nm as indicated by dotted lines. (b) Maximum, minimum, and median values of the UV cure depth profiles at the upper part of the films within 50 nm.

The depth dependent UV curing may help to rationalize the insensitivity of the cohesive fracture resistance to the UV curing. As shown in Fig. 7, several planes of minimum UV cure intensity could exist in an organosilicate film by the standing wave effects, resulting in suppressed UV curing on the film cohesive fracture resistance. The crack path selection[10,11] may facilitate the crack growth along the weakest fracture path in the glass network.

The depth dependent UV curing also help to rationalize the initial film thickness dependence of UV curing effects on adhesive fracture energies observed with FPB tests. Model predictions of UV$\times$10 cure depth profiles for organosilicate films with various initial thicknesses [Fig. 8(a)] are in excellent agreement with the previously reported experimental results[2] in several aspects. First, fracture energies at the upper organosilicate interface are significantly larger than those at the lower interface. Second, the increment in fracture energies at the lower interface increases almost linearly with the decreasing initial film thickness. Third, the increment in fracture energies at the upper interface increases generally for the thinner film with a certain irregularity. The irregularity is thought to be associated with the increasing variation in the UV cure intensity amplitude that the upper part of thinner film would suffer. Figure 8(b) clearly shows that the median value of the UV cure profile at the upper part of the films within 50 nm increases for the thinner films. However, the variation in the UV cure profile also increases precipitously with the decreasing initial film thickness. For example, the variation in the initially 200 nm thick film is 705% larger than that in the initially 800 nm thick films.

The standing wave simulation can predict the depth profiles of broadband UV curing as well as monochromatic UV curing. The broadband UV lamps are usually designed to

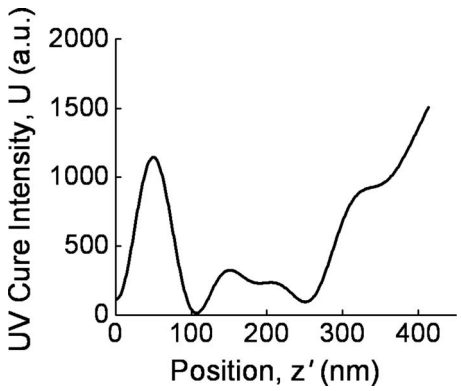

FIG. 9. A simulation prediction of an UV cure depth profile resulting from the superposition of two wavelengths, $\lambda = 254$ and 365 nm.

have several or many prominent wavelengths that involve specific photochemical reactions. For example, shorter wavelengths (<250 nm) can be used to promote cross linking of the silicon backbone, resulting in a harder and stiffer film, whereas longer wavelengths (>250 nm) are designed to accelerate the removal of porogen and the formation of nanometer size pores within the film, leading to a reduction in dielectric constant.[11] The standing waves of each wavelength [Eq. (2)] can be superimposed by the principle of superposition. Figure 9 shows a model prediction of an UV cure depth profile resulting from the superposition of two wavelengths, $\lambda = 254$ and 365 nm. The shape of the UV cure depth profile is very different from those of each wavelength. In theory, all shapes of UV cure depth profiles may be achieved by the superposition of a set of selected wavelengths. Therefore resulting UV cure depth profiles should be taken into account for the selection of specific wavelengths, along with their photochemical reactions, in broadband UV curing. However, superposition of many wavelengths would smooth out the variations, as we have observed with FM-AFM stiffness mapping. Note that the UV cure intensity at the lower interface with a highly reflecting surface is always at a minimum no matter how many wavelengths are superposed. This may explain the insensitivity of adhesive fracture energies at the lower interface to the UV irradiation, not only monochromatic but also broadband [Figs. 2(a) and 2(b)].

An improved understanding of the depth-dependent UV curing effects promises to enable the successful production of ultralow-k (ULK) layers that are multifunctional. Careful selection of the UV spectrum and the underlying layers can result in a cured film with designed depth profiles optimized to have high adhesion and O_2-ashing tolerance at the bottom, ultralow dielectric constant through the film thickness, and high elastic modulus and fracture resistance at the top to endure CMP processing. These multifunctional ULK layers have been achieved with a sequential deposition process involving plasma copolymerization and varying precursor gas flow rates and were considered important for successful integration below 32 nm Cu/ULK nodes.[18] This represents a rather cumbersome processing operation and the technique we described could be achieved in a single-step cure operation.

IV. CONCLUSION

This study demonstrates that UV curing can result in significant depth dependence of the cure. Striking differences between the effects of monochromatic and broadband UV irradiations were observed. For the same as-deposited organosilicate film and cure duration, monochromatic radiation had a greater impact on film structure, elastic modulus, and fracture resistance, but also resulted in a greater degree of depth dependent properties. Oscillating elastic modulus through the film thickness was observed by FM-AFM. We presented a new standing wave model that accurately predicts the resulting depth dependent stiffness variations and can further be used to account for initial film thickness dependence of UV curing and film absorption. We also demonstrated that initial film thickness can have a significant effect on the stiffness cure profile, and further that broadband sources containing multiple peaks can also result in significant depth dependent cure.

ACKNOWLEDGMENTS

The authors acknowledge assistance with sample preparation by Yvonne Ritz of AMD in Dresden. This work was supported by the Director, Office of Energy Research, Office of Basic Energy Sciences, Materials Sciences Division of the U.S. Department of Energy under Contract No. DE-FG02-07ER46391. T.-S. K was supported by ASM Japan K.K.

[1] T. Kim, N. Tsuji, N. Kemeling, K. Matsushita, and R. H. Dauskardt, Proceedings of the Advanced Metallization Conference 2006, 2007 (unpublished), pp. 389–394.
[2] T. Kim, N. Tsuji, N. Kemeling, K. Matsushita, D. Chumakov, H. Geisler, E. Zschech, and R. H. Dauskardt, J. Appl. Phys. **103**, 064108 (2008).
[3] S. Eslava, G. Eymery, P. Marsik, F. Iacopi, C. E. A. Kirschhock, K. Maex, J. A. Martens, and M. R. Baklanov, J. Electrochem. Soc. **155**, G115 (2008).
[4] H. Hertz, J. Reine Angew. Math. **92**, 156 (1882).
[5] R. J. Hohlfelder, D. A. Maidenberg, R. H. Dauskardt, Y. Wei, and J. W. Hutchinson, J. Mater. Res. **16**, 243 (2001).
[6] R. H. Dauskardt, M. Lane, Q. Ma, and N. Krishna, Eng. Fract. Mech. **61**, 141 (1998).
[7] M. F. Kanninen, Int. J. Fract. **9**, 83 (1973).
[8] E. P. Guyer and R. H. Dauskardt, J. Mater. Res. **19**, 3139 (2004).
[9] K. Matsushita, N. Tsuji, K. Kagami, M. Kato, S. Kaneko, and N. Kobayashi, Proceedings of the Advanced Metallization Conference ADMETA 2007, 2007 (unpublished), pp. 258–259.
[10] D. M. Gage, E. P. Guyer, J. F. Stebbins, Z. Cui, A. Al-Bayati, A. Demos, K. P. MacWilliams, and R. H. Dauskardt, IEEE International Interconnect Technology Conference Proceedings 2006 (unpublished), pp. 146–148.
[11] D. M. Gage, J. F. Stebbins, L. Peng, Z. Cui, A. Al-Bayati, K. P. MacWilliams, H. M'Saad, and R. H. Dauskardt, J. Appl. Phys. **104**, 043513 (2008).
[12] E. P. Guyer, M. Patz, and R. H. Dauskardt, J. Mater. Res. **21**, 882 (2006).
[13] N. Kemeling, K. Matsushita, N. Tsuji, K. Kagami, M. Kato, S. Kaneko, H. Sprey, D. d. Roest, and N. Kobayashi, Microelectron. Eng. **84**, 2575 (2007).
[14] C. A. Mack, Appl. Opt. **25**, 1958 (1986).
[15] F. H. Dill, IEEE Trans. Electron Devices **22**, 440 (1975).
[16] F. H. Dill, A. R. Neureuther, J. A. Tuttle, and E. J. Walker, IEEE Trans. Electron Devices **22**, 456 (1975).
[17] J. D. Cuthbert, Solid State Technol. **50**, 59 (1977).
[18] M. Tada, H. Yamamoto, F. Ito, M. Narihiro, M. Ueki, N. Inoue, M. Abe, S. Saito, T. Takeuchi, N. Furutake, T. Onodera, J. Kawahara, K. Arai, Y. Kasama, T. Taiji, M. Tohara, M. Sekine, and Y. Hayashi, Proceedings of the International Electron Devices Meeting 2006, 2006 (unpublished), p. 346781.